Robust Sparse Fourier Transform Based on The Fourier Projection-Slice Theorem

Shaogang Wang, Vishal M. Patel and Athina Petropulu
Department of Electrical and Computer Engineering
Rutgers, the State University of New Jersey, Piscataway, NJ 08854, USA

***Abstract*—We have recently proposed a sparse Fourier transform based on the Fourier projection-slice theorem (FPS-SFT), which is an efficient implementation of the discrete Fourier transform for multidimensional signals that are sparse in the frequency domain. For a K-sparse signal, FPS-SFT achieves sample complexity of $O(K)$ and computational complexity of $O(K \log K)$. While FPS-SFT considers the ideal scenario, i.e., exactly sparse data that contain on-grid frequencies, in this paper, we propose a robust FPS-SFT (RFPS-SFT), which applies to noisy signals that contain off-grid frequencies; such signals arise in radar applications. RFPS-SFT employs a windowing step and a voting-based frequency decoding step; the former reduces the frequency leakage of off-grid frequencies below the noise level, thus preserving the sparsity of the signal, while the latter significantly lowers the frequency localization error stemming from the noise. The performance of the proposed method is demonstrated both theoretically and numerically.**

***Index Terms*—Multidimensional signal processing, sparse Fourier transform, automotive radar, projection-slice theorem.**

I. Introduction

With the rapid development of advanced driver-assistance systems (ADAS) and self-driving cars, automotive radars play an increasingly important role in providing multidimensional information about the dynamic environment to the control unit of the car. Traditional automotive radars use frequency modulation continuous waveforms (FMCW) to measure range and range rate (Doppler) of targets, such as cars, pedestrians and obstacles. A digital beamforming (DBF) automotive radar [1] can provide target angular information both in azimuth and elevation [2], which is desirable in the ADAS and self-driving applications.

A typical DBF automotive radar uses a uniform linear array (ULA) as receive array. For such configuration and under the narrow-band signal assumption, each radar target can be represented by a D-dimensional (D-D) complex sinusoid [3], whose frequency in each dimension is related to target range, Doppler and direction of arrival (DOA). Simultaneous multidimensional parameter estimation of a DBF automotive radar requires intensive computations. The conventional implementation relies on a D-D discrete Fourier transform (DFT), which can be implemented by the fast Fourier transform (FFT). The sample complexity of the FFT is $O(N)$, where $N = \prod_{i=0}^{D-1} N_i$ is the number of samples in the D-D data cube with N_i the sample length for the i-th dimension. For N a power of 2, the computational complexity of the FFT is $O(N \log N)$. Since N is typically large, the processing via FFT is still demanding for real-time processing.

The recently proposed sparse Fourier transform (SFT) [4]–[6] leverages the sparsity of signals in the frequency domain to reduce the sample and computational complexity of DFT. Different versions of the SFT have been investigated in various applications including medical imaging [7], and radar signal processing [8]. In radar signal processing, the number of radar targets, K, is usually much smaller than N, which makes the radar signal sparse in the D-D frequency domain. Hence, it is tempting to replace the FFT with SFT in order to reduce the complexity of radar signal processing. However, most of the SFT algorithms are designed for 1-dimensional (1-D) signals, while their extension to multidimensional signals is usually not straightforward. This is because the SFT algorithms are not separable in each dimension since operations such as detection within an SFT algorithm must be considered jointly for all the dimensions [8].

Multidimensional SFT algorithms are investigated in [7], [9], [10]; those algorithms share a the same idea, i.e., reduction of a multidimensional DFT into a number of 1-D DFTs. The SFT of [9] achieves the sample and computational complexity lower bounds of all known SFT algorithms by reducing a 2-dimensional (2-D) DFT into 1-D DFTs, computed along a few rows and columns of a data matrix. However, such algorithm requires a very sparse frequency domain signal, whose frequencies are uniformly distributed. Such limitation stems from the restriction of applying DFT only along axes of the data matrix; this corresponds to projecting the 2-D DFT onto its two axes. In [7], [10], the multidimensional DFT is implemented via 1-D DFTs taken on samples along a few lines extracted from the multidimensional data; those lines are parameterized by predefined, deterministic slopes. Although employing lines with various slopes leads to more degrees of freedom for frequency projection of the DFT domain, the limited choice of line slopes in [7], [10] is still an obstacle in addressing less sparse signals. Moreover, the localization of frequencies in [7], [10] is not as efficient as that of [9]. The latter recovers the significant frequencies in an *iterative* manner; the contribution of the recovered frequencies is removed from the signal, creating a sparser signal for the future iterations, while the former recover all frequencies in *one-shot* based on a voting procedure, which involves higher complexity.

We have recently proposed FPS-SFT [11], a multidimen-

sional, Fourier projection-slice based SFT, which enjoys low complexity while avoiding the limitations of the aforementioned algorithms, i.e., it can handle less sparse data in the frequency domain, with frequencies that are non-uniformly distributed. FPS-SFT uses the low-complexity frequency localization framework of [9], and extends the multiple slopes idea of [7], [10] by using lines of randomly runtime-generated slopes. The randomly selected line slopes enables large degrees of freedom in frequency projection in FPS-SFT. Thus, less sparse, non-uniformly distributed frequencies can be effectively resolved. Employing random lines is not trivial, since the line parameters, including line length and set of slopes should be carefully designed to enable orthogonal and uniform frequency projection (see Lemmas 1 and 2 in [11]). FPS-SFT can be viewed as a low-complexity, Fourier projection-slice approach for signals that are sparse in the frequency domain. In FPS-SFT, the DFT of an 1-D slice of the D-D data is the projection of the D-D DFT on that line. While the classical Fourier projection-slice based method reconstructs the frequency domain representation of the signal via interpolation of frequency-domain slices, the FPS-SFT aims to reconstruct the frequency-domain signal directly based on frequency domain projections; this is achieved by leveraging the sparsity of the signal in the frequency domain.

FPS-SFT of [11] considers the case with exactly sparse data containing frequencies on the grid, while suffers from frequency leakage when the data contains off-grid frequencies. Also, its frequency localization, based on the so-called OFDM-trick [4], is prone to errors when the signal contains noise. We propose robust FPS-SFT (RFPS-SFT), a scheme that addresses both aforementioned shortcomings, therefore, makes the FPS-SFT more applicable to realistic radar applications where the radar signal contains off-grid frequencies and noise.

The off-grid frequencies are also addressed in [8], where we proposed a robust multidimensional SFT algorithm, i.e., RSFT. In RSFT, the computational savings are achieved by folding the input D-D data cube into a much smaller data cube, on which a reduced sized D-D FFT is applied. Although the RSFT is more computationally efficient as compared to the FFT-based methods, its sample complexity is the same as the FFT-based algorithms. Essentially, the high sample complexity of RSFT is due to its two stages of windowing procedures, which are applied to the entire data cube to suppress the frequency leakage. Inspired by RSFT, the windowing technique is also applied in the RFPS-SFT to address the frequency leakage problem, caused by off-grid frequencies. However, instead of applying the multidimensional window on the entire data as in the RSFT, the window is still designed for the full-sized data, but is applied only on samples along lines; this does not cause overhead in sample complexity. To address the frequency localization problem in FPS-SFT stemming from noise, RFPS-SFT employs a voting-based frequency localization procedure, which significantly lowers the localization error. The performance of RFPS-SFT is demonstrated both theoretically and numerically, and the feasibility of RFPS-SFT in automotive radar signal processing is shown via simulations.

Notation: We use lower-case (upper-case) bold letters to denote vectors (matrix). $[\cdot]^T$ denotes the transpose of a vector. The N-modulo operation is denoted by $[\cdot]_N$, while the 1-modulo operation is denoted by $[\cdot]_1$. $[S]$ refers to the integer set of $\{0, ..., S-1\}$. The cardinality of set $\mathbb{S}$ is denoted as $|\mathbb{S}|$. The DFT of signal x is denoted by $\hat{x}$. $\|\mathbf{W}\|_1, \|\mathbf{W}\|_2$ are the l_1 and l_2 norm of matrix $\mathbf{W}$, respectively.

II. Signal Model and Problem Formulation

We consider a radar configuration that employs a ULA as the receive array. Assume that the ULA has N_1 half-wavelength-spaced elements. The radar transmits a FMCW waveform with repetition interval (RI) T_p. We assume that there exist K targets in the radar coverage. After de-chirping, sampling and analog-to-digital conversion for both I and Q channels, the received signal within an RI can be expressed as a superposition of K 2-D complex sinusoids in noise [3], i.e.,

$$r(\mathbf{n}) = y(\mathbf{n}) + n(\mathbf{n}) = \sum_{(a,\boldsymbol{\omega})\in\mathbb{S}} a e^{j\mathbf{n}^T\boldsymbol{\omega}} + n(\mathbf{n}), \tag{1}$$

where $\mathbf{n} \triangleq [n_0, n_1]^T \in \mathcal{X} \triangleq [N_0] \times [N_1]$ is the sampling grid and N_0 is the number of samples within an RI. $y(\mathbf{n}) \triangleq \sum_{(a,\boldsymbol{\omega})\in\mathbb{S}} a e^{j\mathbf{n}^T\boldsymbol{\omega}}$ is the signal part of the received signal; $(a, \boldsymbol{\omega})$ represents a 2-D frequency, whose complex amplitude is a, and it holds that $0 < a_{min} \leq |a| \leq a_{max}$; the 2-D frequency $\boldsymbol{\omega} \triangleq [\omega_0, \omega_1]^T \in [0, 2\pi)^2$ represents the normalized radian frequencies corresponding to targets' range and DOA, respectively. The set $\mathbb{S}$, with $|\mathbb{S}| = K$ contains all the 2-D frequencies. The noise, $n(\mathbf{n})$, is assumed to be i.i.d., circularly symmetric Gaussian, i.e., $\mathcal{CN}(0, \sigma_n)$. The SNR of a sinusoid with amplitude a is defined as $SNR \triangleq (|a|/\sigma_n)^2$.

The target's range r, Doppler f_d and DOA θ are related to $\boldsymbol{\omega}$ as $\omega_0 = 2\pi(2\rho r/c + f_d)/f_s, \omega_1 = \pi \sin\theta$, where ρ, c, f_s are the chirp rate, speed of wave propagation and sampling frequency, respectively; the chirp rate is defined as the ratio of the signal bandwidth and the RI. Thus, the target parameters are embedded in frequencies ω_0, ω_1, which can detected in the 2-D $N_0 \times N_1$-point DFT of the windowed $r(\mathbf{n})$ [3], i.e.,

$$\begin{aligned}\hat{r}(\mathbf{m}) &\triangleq \frac{1}{N}\sum_{\mathbf{n}\in\mathcal{X}} w(\mathbf{n}) r(\mathbf{n}) e^{-j2\pi\left(\frac{m_0 n_0}{N_0} + \frac{m_1 n_1}{N_1}\right)}, \\ &= \hat{y}(\mathbf{m}) + \hat{n}(\mathbf{m}),\ \mathbf{m} \triangleq [m_0, m_1]^T \in \mathcal{X},\end{aligned} \tag{2}$$

where $w(\mathbf{n})$ is a 2-D window, introduced to suppress frequency leakage generated by off-grid frequencies; $N = N_0 N_1$; and $\hat{y}(\mathbf{m}), \hat{n}(\mathbf{m})$ are the DFTs of the windowed $y(\mathbf{n})$ and $n(\mathbf{n})$, respectively. Assuming that the peak to side-lobe ratio (PSR) of the window is large enough, such that the side-lobe of each frequency in $\mathbb{S}$ can be neglected in the DFT domain, the signal contribution in the DFT domain can be viewed as a set of on-grid frequencies, i.e., $\mathbb{S}' \triangleq \{(a, \boldsymbol{\omega}) : \boldsymbol{\omega} \triangleq [2\pi m_0/N_0, 2\pi m_1/N_1]^T, [m_0, m_1]^T \in \mathcal{X}\}$ with $K < |\mathbb{S}'| << N$. Hence, $x(\mathbf{n})$, the sample domain signal

component associated with the window $w(\mathbf{n})$ and $\mathbb{S}'$ can be approximated by

$$x(\mathbf{n}) \triangleq \sum_{(a,\boldsymbol{\omega})\in\mathbb{S}'} a e^{j2\pi\left(\frac{m_0 n_0}{N_0}+\frac{m_1 n_1}{N_1}\right)},\ [n_0,n_1]^T \in \mathcal{X}. \quad (3)$$

Note that since the windowing degrades the frequency resolution, each continuous-valued frequency in $\mathbb{S}$ is related to a cluster of digital frequencies in $\mathbb{S}'$; $\mathbb{S}'$ can be estimated from the DFT of the signal, and then lead to the frequencies in $\mathbb{S}$ via quadratic interpolation [12].

The state-of-the-art DBF automotive radars also measure target Doppler f_d by processing a 3-dimensional (3-D) data cube, generated based on N_2 consecutive RIs [3]. The normalized radian frequency ω_2 in the Doppler dimension is related to the Doppler as $\omega_2 = 2\pi f_d T_p$. The DBF automotive radars that also measure elevation DOA introduce a 4-th dimension of processing [2]; the DOA measurement in elevation is similar to that of the azimuth DOA dimension. In those cases, the proposed RFPS-SFT algorithm can be naturally extended to multidimensional cases, where the reduction of complexity of the signal processing algorithms is more significant.

III. The RFPS-SFT Algorithm

The FPS-SFT algorithm proposed in [11] applies to multidimensional data of arbitrary size that is exactly sparse in the frequency domain. In the 2-D case, FPS-SFT implements a 2-D DFT as a series of 1-DFTs on samples taken along lines, with each line being parameterized by the random slope parameters $\boldsymbol{\alpha} \triangleq [\alpha_0,\alpha_1]^T \in \mathcal{X}$ and delay parameters $\boldsymbol{\tau} \triangleq [\tau_0,\tau_1]^T \in \mathcal{X}$. The signal along such line can be expressed as

$$\begin{aligned} s(\boldsymbol{\alpha},\boldsymbol{\tau},l) &\triangleq x([\alpha_0 l+\tau_0]_{N_0},[\alpha_1 l+\tau_1]_{N_1}) \\ &= \sum_{(a,\boldsymbol{\omega})\in\mathbb{S}'} a e^{j2\pi\left(\frac{m_0[\alpha_0 l+\tau_0]_{N_0}}{N_0}+\frac{m_1[\alpha_1 l+\tau_1]_{N_1}}{N_1}\right)}, l\in[L]. \end{aligned} \quad (4)$$

Taking an L-point DFT on (4), for $m \in [L]$, we get

$$\begin{aligned} \hat{s}(\boldsymbol{\alpha},\boldsymbol{\tau},m) &\triangleq \frac{1}{L}\sum_{l\in[L]} s(\boldsymbol{\alpha},\boldsymbol{\tau},l) e^{-j2\pi\frac{lm}{L}} \\ &= \frac{1}{L}\sum_{(a,\boldsymbol{\omega})\in\mathbb{S}'} a e^{j2\pi\left(\frac{m_0\tau_0}{N_0}+\frac{m_1\tau_1}{N_1}\right)} \sum_{l\in[L]} e^{j2\pi l\left(\frac{m_0\alpha_0}{N_0}+\frac{m_1\alpha_1}{N_1}-\frac{m}{L}\right)}. \end{aligned} \quad (5)$$

Let us assume that for all $m \in [L], [m_0,m_1]^T \in \mathcal{X}$,

$$\hat{f}(m) \triangleq \frac{1}{L}\sum_{l\in[L]} e^{j2\pi l\left(\frac{m_0\alpha_0}{N_0}+\frac{m_1\alpha_1}{N_1}-\frac{m}{L}\right)} \in \{0,1\}. \quad (6)$$

This holds when $\frac{m_0\alpha_0}{N_0}+\frac{m_1\alpha_1}{N_1}-\frac{m}{L}$ is multiple of $1/L$, which requires the line length L to be the least common multiple (LCM) of N_0, N_1 (see Lemma 1 of [11]).

When $\hat{f}(m) = 1$, i.e.,

$$\left[\frac{m_0\alpha_0}{N_0}+\frac{m_1\alpha_1}{N_1}-\frac{m}{L}\right]_1 = 0, [m_0,m_1]^T \in \mathcal{X}, \quad (7)$$

(5) can be simplified as $\hat{s}(\boldsymbol{\alpha},\boldsymbol{\tau},m) = \sum_{(a,\boldsymbol{\omega})\in\mathbb{S}} a e^{j2\pi\left(\frac{m_0\tau_0}{N_0}+\frac{m_1\tau_1}{N_1}\right)}$.

The solutions of (7) with respect to m are equally spaced points $[m_0,m_1]^T$ that lie on a line with slope $-\alpha_0 N_1/(\alpha_1 N_0)$ in the $N_0 \times N_1$-point DFT domain (see the proof of Lemma 2 in [11]), and it holds that

$$m_0 = [m_0' + k\alpha_1 L/N_1]_{N_0}, m_1 = [m_1' - k\alpha_0 L/N_0]_{N_1}, k\in\mathbb{Z}, \quad (8)$$

where $[m_0',m_1']^T \in \mathcal{X}$ is one of the solutions of (7).

Hence each entry of the L-point DFT of the slice taken along a time-domain line with slope α_1/α_0 represents a projection of the 2-D DFT along the line with slope $-\alpha_0 N_1/(\alpha_1 N_0)$, which is orthogonal to the time-domain line. This is closely related to the Fourier projection-slice theorem. In fact, FPS-SFT can be viewed as a low-complexity, Fourier projection-slice based multidimensional DFT. This is achieved by exploring the sparse nature of the signal in the frequency domain, as explained in the following.

We apply the assumption that the signal is sparse in the frequency domain; specifically, we assume that $|\mathbb{S}'| = O(L)$. Then, if $|\hat{s}(\boldsymbol{\alpha},\boldsymbol{\tau},m)| \neq 0$, with high probability, the m-th bin is 1-sparse, and it holds that $\hat{s}(\boldsymbol{\alpha},\boldsymbol{\tau},m) = a e^{j2\pi\left(\frac{m_0\tau_0}{N_0}+\frac{m_1\tau_1}{N_1}\right)}, (a,\boldsymbol{\omega}) \in \mathbb{S}'$. In such case, the 2-D frequency, $(a,\boldsymbol{\omega})$, can be 'decoded' using three lines of the same slope but different offsets, i.e., $\boldsymbol{\tau},\boldsymbol{\tau}_0 \triangleq [[\tau_0+1]_{N_0},\tau_1]^T, \boldsymbol{\tau}_1 \triangleq [\tau_0,[\tau_1+1]_{N_1}]^T$, respectively. Such design allows the frequencies to be decoded independently in each dimension. The frequency corresponding to the 1-sparse bin, m, can be decoded as

$$\begin{aligned} m_0 &= \left[\frac{N_0}{2\pi}\phi\left(\frac{\hat{s}(\boldsymbol{\alpha},\boldsymbol{\tau}_0,m)}{\hat{s}(\boldsymbol{\alpha},\boldsymbol{\tau},m)}\right)\right]_{N_0}, \\ m_1 &= \left[\frac{N_1}{2\pi}\phi\left(\frac{\hat{s}(\boldsymbol{\alpha},\boldsymbol{\tau}_1,m)}{\hat{s}(\boldsymbol{\alpha},\boldsymbol{\tau},m)}\right)\right]_{N_1}, \\ a &= \hat{s}(\boldsymbol{\alpha},\boldsymbol{\tau},m) e^{-j2\pi(m_0\tau_0/N_0+m_1\tau_1/N_1)}. \end{aligned} \quad (9)$$

In order to recover all the frequencies in $\mathbb{S}'$ efficiently, each iteration of FPS-SFT adopts a random choice of line slope (see Lemma 2 of [11]) and offset. Furthermore, the contribution of the recovered sinusoids in the previous iterations is removed via a *construction-subtraction* approach so that the signal becomes sparser in future iterations. Specifically, assuming that for the current iteration the line slope and offset parameters are $\boldsymbol{\alpha},\boldsymbol{\tau}$, respectively, the recovered 2-D frequencies are projected into L frequency bins to construct the DFT along the corresponding line, i.e., $\hat{s}_r(\boldsymbol{\alpha},\boldsymbol{\tau},m) \triangleq \sum_{(a,\boldsymbol{\omega})\in\mathcal{I}_m} a e^{j2\pi\left(\frac{m_0\tau_0}{N_0}+\frac{m_1\tau_1}{N_1}\right)}$, $m\in[L]$, where $\mathcal{I}_m, m\in[L]$ represent the subsets of the recovered frequencies, i.e., $\mathcal{I}_m \triangleq \{(a,\boldsymbol{\omega}) : [\frac{m_0\alpha_0}{N_0}+\frac{m_1\alpha_1}{N_1}-\frac{m}{L}]_1 = 0, [m_0,m_1]^T \in \mathcal{X}\}, m\in[L]$. Next, the L-point inverse DFT (IDFT) is applied on $\hat{s}_r(\boldsymbol{\alpha},\boldsymbol{\tau},m), m\in[L]$, from which the line, $s_r(\boldsymbol{\alpha},\boldsymbol{\tau},l), l\in[L]$ due to the previously recovered frequencies is constructed. Subsequently, the line points are subtracted from the signal samples of the current iteration.

A. RFPS-SFT

FPS-SFT [11] is developed for data that is exactly sparse in the frequency domain. Also, the frequencies are assumed to be on the DFT grid. In the radar application however, the radar signal contains noise. Also, the discretized frequencies associated with target parameters are typically off-grid. In the following, we propose RFPS-SFT, which employs the windowing technique to reduce the frequency leakage produced by the off-grid frequencies and a voting-based frequency localization to reduce the frequency decoding error due to noise.

1) Windowing: To address off-grid frequencies we apply a window $w(\mathbf{n}), \mathbf{n} \in \mathcal{X}$ on the signal of (1). The PSR of the window, ρ_w, is designed such that the side-lobes of the *strongest* frequency are below the noise level, hence the leakage of the significant frequencies can be neglected and the sparsity of the signal in the frequency domain can be preserved to some extend. The window design requires the knowledge of the SNR of the strongest sinusoids contained in the signal, which can be assumed *a priori* or obtained via estimation in real-life applications. The following lemma reflects the relationship between ρ_w and the maximum SNR of the signal.

Lemma 1. ***(Window Design):*** *Consider (2), which is the $N_0 \times N_1$-point DFT of signal of (1). Let $\mathbf{W} \in \mathbb{R}^{N_0 \times N_1}$ be the matrix generated by the window function $w(\mathbf{n}), \mathbf{n} \in \mathcal{X}$. The PSR of the window, ρ_w, should be designed such that*

$$\rho_w > \frac{2\|\mathbf{W}\|_1}{\sqrt{\pi}\|\mathbf{W}\|_2}\sqrt{SNR_{max}}, \tag{10}$$

Where $SNR_{max} \triangleq a_{max}^2/\sigma_n^2$.

Note that unlike the RSFT that applies windows on the entire data cube, in RFPS-SFT, while the window is still designed for the entire data cube, the windowing is applied only on the sampled locations. Thus, the windowing does not increase the sample and computational complexity of RFPS-SFT.

2) Voting-based frequency decoding: When the signal is approximately sparse, i.e., the signal spectrum is dominated by $K, K << N$ frequencies, the frequencies decoded by (9) are not integers. Since we aim to recover the gridded frequencies, i.e., $\mathbb{S}'$ of (3), the recovered frequencies are rounded to the nearest integers. When the SNR is low, the frequency decoding could result into false frequencies; those false frequencies enter the future iterations and generate more false frequencies. To suppress the false frequencies, motivated by the classical m-out-of-n radar signal detector [13], RFPS-SFT adopts an n_d-out-of-n_s voting procedure in each iteration. Specifically, within each iteration of RFPS-SFT, n_s sub-iterations are applied; each sub-iteration adopts randomly generated line slope and offset parameters and recovers a subset of frequencies, $\mathbb{S}_i, i \in [n_s]$. Within those frequency sets, a given frequency could be recovered by n out of n_s sub-iterations. For a true significant frequency, n is typically larger than that of a false frequency, thus only those frequencies with $n \geq n_d$ are retained as the recovered frequencies of the current iteration. When (n_s, n_d) are properly chosen, the false frequencies can be reduced significantly.

3) Lower bound of the probability of correct localization and convergence of RFPS-SFT: The probability of decoding error relates to the SNR, signal sparsity and choice of (n_s, n_d) in RFPS-SFT. In the following, we provide the lower bound for the probability of correct localization of the significant frequencies for each iteration of RFPS-SFT, from which one can derive the number of iterations of RFPS-SFT in order to recover all the significant frequencies of sufficient SNR.

According to Section II, a 2-D sinusoid $(a, \boldsymbol{\omega}) \in \mathbb{S}$ of (1) is associated with a cluster of 2-D sinusoids $\mathbb{S}_0 \subseteq \mathbb{S}'$ of (3), whose frequencies are on the grid of the $N_0 \times N_1$-point DFT. Let us assume that the sinusoid $(a_d, 2\pi[m_0/N_0, m_1/N_1]^T) \in \mathbb{S}_0$ with $[m_0, m_1]^T \in \mathcal{X}$ has the largest absolute amplitude among the sinusoids in $\mathbb{S}_0$. Assuming that the SNR of $(a, \boldsymbol{\omega})$ is sufficiently high, the probability of correctly localizing $[m_0, m_1]^T$ in each iteration of RFPS-SFT is lower bounded by

$$P_d \triangleq \sum_{n_d'=n_d}^{n_s} \binom{n_s}{n_d'} (P_1 P_w)^{n_d'} (1 - P_1 P_w)^{n_s - n_d'}, \tag{11}$$

where $P_1 \triangleq (1 - |\mathbb{S}''|/N)^{N/L-1}$ with $L = \mathrm{LCM}(N_0, N_1)$ is the probability of a sinusoid in $\mathbb{S}''$ being projected to a 1-sparse bin, and $\mathbb{S}''$ with $\mathbb{S}'' \subseteq \mathbb{S}'$ represents the remaining sinusoids to be recovered in the future iterations of RFPS-SFT; $P_w \triangleq (1-P_u)(1-P_v)$ is the lower bound of the probability of correct localization for a 2-D sinusoid that is projected into a 1-sparse bin for one sub-iteration of RFPS-SFT; P_u, P_v are the upper bounds of the probability of localization error for the two frequency components, m_0, m_1, respectively, which is defined as $P_u \triangleq \left(\sigma_p(1 - f_{|a_n|}(\delta_u))\right)^2, P_v \triangleq \left(\sigma_p(1 - f_{|a_n|}(\delta_v))\right)^2$, where $\delta_u \triangleq a\pi\|\mathbf{W}\|_1/(2NN_0)$, $\delta_v \triangleq a\pi\|\mathbf{W}\|_1/(2NN_1)$, with $\mathbf{W} \in \mathbb{R}^{N_0 \times N_1}$ the window that is applied on the data; σ_p with $\frac{1}{2} \leq \sigma_p \leq \frac{1}{2\pi}$ is the parameter determined by the phases of the error vectors contained in the 1-sparse bin; $f_{|a_n|}(x)$ is the cumulative distribution function (CDF) of the Rayleigh distribution, which is defined as $f_{|a_n|}(x) \triangleq 1 - e^{-x^2/(2\sigma_{a_n'}^2)}$, $x > 0$, where $\sigma_{a_n'}^2 \triangleq \sigma_n^2\|\mathbf{W}\|_2^2/(2NL)$. The Rayleigh distribution arises from the amplitude of the complex Gaussian noise.

Essentially, (11) represents the complementary cumulative binomial probability resulted from the n_d-out-of-n_s voting procedure, where the success probability of each experiment, i.e., localizing $(a_d, 2\pi[m_0/N_0, m_1/N_1]^T)$ in each sub-iteration of RFPS-SFT is $P_1 P_w$. When $|\mathbb{S}'|$ is known, (11) can be applied to estimate the largest number of iterations (the upper bound) of RFPS-SFT in order to recover all the significant sinusoids in $\mathbb{S}'$ since the least number of recovered sinusoids in each iteration can be estimated by $|\mathbb{S}''|P_d$.

4) Multidimensional extension: The multidimensional extension of RFPS-SFT is straightforward and similar to that of FPS-SFT (See Section 2.3 of [11] for details).

5) Complexity analysis: The RFPS-SFT executes T iterations; within each iteration, n_s sub-iterations with ran-

domized line parameters are invoked. The samples used in each sub-iteration is $3L$, since three L-length lines, with $L = \text{LCM}(N_0, N_1)$ are extracted to decode the two frequency components in the 2-D case. Hence, the sample complexity of RFPS-SFT is $O(3Tn_sL) = O(L)$.

The core processing of RFPS-SFT is the L-point DFT, which can be implemented by the FFT with computational complexity of $O(L \log L)$. In addition to the FFT, each sub-iteration needs to evaluate $O(|\mathbb{S}'|)$ frequencies. Hence the computational complexity of RFPS-SFT is $O(L \log L + |\mathbb{S}'|)$. Assuming that $|\mathbb{S}'| = O(L)$, the sample and computational complexity can be simplified as $O(|\mathbb{S}'|)$ and $O(|\mathbb{S}'| \log |\mathbb{S}'|)$, respectively. Furthermore, since $K = O(|\mathbb{S}'|)$, the sample and computational complexity of RFPS-SFT can be further simplified as $O(K)$ and $O(K \log K)$, respectively.

Generally, in the D-D case, according to the multidimensional extension, it is easy to see that the sample and computational complexity of RFPS-SFT are $O(DK)$ and $O(DK \log(DK))$, respectively, when $K = O(L)$.

IV. Numerical Results

Effect of windowing on frequency localization: For the data that contains off-grid frequencies, the PSR of the required window is given in Lemma 1. However, the larger the PSR, the wider the main-lobe of the window, which results into larger frequency clusters in the DFT domain and thus larger $|\mathbb{S}'|$ (see (3)), i.e., a less sparse signal. Moreover, the larger the PSR, the smaller the SNR of the windowed signal, which leads to larger frequency localization error. Hence, for a signal with known maximum SNR, SNR_{max}, there exists a window with the optimal PSR in terms of frequency localization success rate, i.e., ratio of number of correctly localized frequencies to the number of significant frequencies, which is $|\mathbb{S}'|$ in one iteration of RFPS-SFT. Fig. 1 shows the numerical evaluation of such optimal windows for signals for various values of SNR_{max} and sparsity level, i.e., $K = |\mathbb{S}|$. According to (10), for signals with SNR_{max} equal to $20dB$ and $30dB$, the PSR of the window should be larger than $56dB$ and $60dB$, respectively. The corresponding optimal PSR for the Dolph-Chebyshev windows appear to be $60dB$ and $70dB$, respectively. Fig. 1 shows the success rate of the first iteration of RFPS-SFT, which is the lowest success rate of all the iterations.

Fig. 2 demonstrates localization of off-grid 2-D frequencies of RFPS-SFT using Dolph-Chebyshev window for various values of PSR. A windows with insufficient PSR leads to miss detections and false alarms (see Fig. 2 (a)), while a window with sufficiently large PSR yields good performance in frequency localization, with a trade-off of causing larger frequency cluster sizes (see Fig. 2 (b)).

Effect of voting on frequency localization: The n_d-out-of-n_s voting in frequency decoding procedure of RFPS-SFT can significantly reduce the false alarm rate. A low false alarm rate in each iteration of RFPS-SFT is required since the false frequencies would enter the next iteration of RFPS-SFT, which creates more false frequencies. For a fixed n_s, the larger the n_d/n_s is, the smaller the false alarm rate is. However, this involves a trade-off between false alarm rate and complexity; specifically, the smaller the false alarm rate, the larger the number of the iterations required to recover all the significant frequencies.

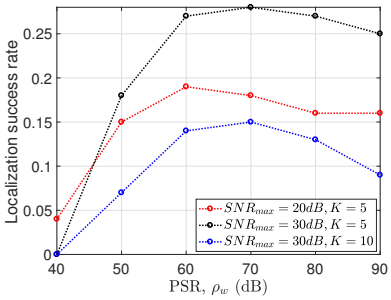

Fig. 1. Frequency localization success rate of the first iteration of RFPS-SFT versus window PSR. The Dolph-Chebyshev windows with various PSR is applied. $N_0 = N_1 = 256; (n_s, n_d) = (3, 2)$. The results are averaged based on 100 iterations of Monte Carlo simulation.

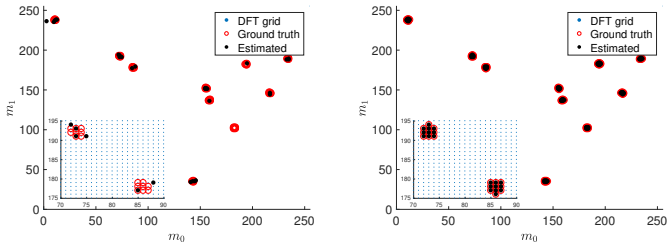

(a) (b)

Fig. 2. 2-D frequency recovery with different window. $K = 10, \sigma_n = 1, a_{min} = a_{max}, SNR_{max} = 30dB, (n_s, n_d) = (3, 2), T = 30$. Dolph-Chebyshev windows with various PSR are adopted. The ground truth represents $\mathbb{S}'$ of (3), which relates to the window. (a) $\rho_w = 45dB$. (b) $\rho_w = 70dB$.

Figs. 3 and Fig. 2 (b) show the examples of 2-D frequency recovery using different (n_s, n_d). In Fig. 3 (a), we set $(n_s, n_d) = (1, 1)$, which reduces to the frequency localization in FPS-SFT, i.e., without voting. In this case, one can see that many false frequencies are generated. Figs. 3 (b) and Fig. 2 (b) show the frequency localization result with (n_s, n_d) equal to $(3, 1)$ and $(3, 2)$, respectively; while the former generates large amount of false frequencies, the latter exhibits ideal performance.

Effect of the SNR and the sparsity level on the number of iterations of RFPS-SFT: The number of iterations of RFPS-SFT to recover all the significant frequencies is affected by the SNR and the sparsity level of the signal. A low SNR and less sparse signal requires large number of iterations. As discussed in Section III-A3, we are able to estimate the largest number of iterations that recovers $\mathbb{S}'$. Figs. 4 (a) shows the predicted and measured number of recovered frequencies in each iteration of RFPS-SFT for $|\mathbb{S}'|$ equal to 1000. Fig. 4 (b) shows the predicted and measured number of iterations of RFPS-SFT for signal with various SNR and sparsity level. The figure shows that the number of iterations upper bounds are consistent with the measurements.

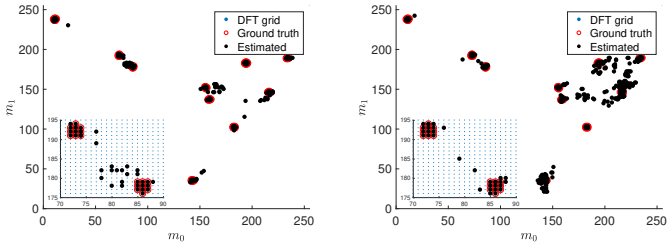

(a) (b)

Fig. 3. Effect of voting on 2-D frequency recovery. $K = 10, \sigma_n = 1, a_{min} = a_{max}, SNR_{max} = 30dB$. $T = 30$ for (a)-(c). Dolph-Chebyshev windows with $\rho_w = 70dB$ is applied. The n_d-out-of-n_s voting procedure significantly improves frequency localization performance when (n_d, n_s) is properly designed. (a) $(n_d, n_s) = (1, 1)$. (b) $(n_d, n_s) = (3, 1)$.

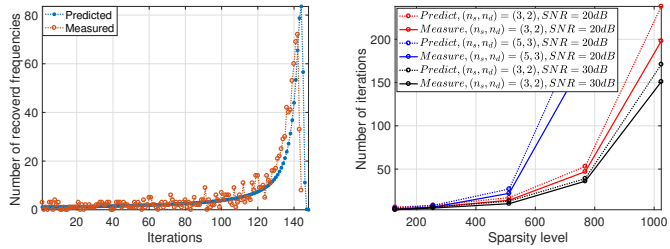

(a) (b)

Fig. 4. Effect of SNR and sparsity level on number of iterations of RFPS-SFT. (a) $|\mathbb{S}|' = 1000, SNR = 30dB, \sigma_p = 1/6$. (b) Comparison of predicted and measured number of iterations for various SNR and sparsity level, $|\mathbb{S}'|$.

TABLE I
RADAR PARAMETERS

Parameter	Symbol	Value
Center frequency	f_c	$76GHz$
Pulse bandwidth	b_w	$200MHz$
Pulse repetition time	T_p	$89us$
Number of range bins	N_0	512
Number of PRI	N_1	256
Number of antenna elements	N_2	16
Maximum range	R_{max}	$300m$

Radar target reconstruction: We simulate the target reconstruction for a DBF automotive radar via RFPS-SFT and compare with the RSFT. The main radar parameters are listed in Table I; such radar configuration represents a typical long-range DBF radar [3] except that we set the number of antenna elements to be moderately large to provide a better angular measurement performance. Fig. 5 shows the target reconstruction of 3 radar targets via 3-D FFT, RFPS-SFT and RSFT. All the three algorithms are able to reconstruct all the targets. Compared to the FFT and RSFT, RFPS-SFT only requires approximately 3% of data samples, which exhibits low sample complexity. However, we note that RFPS-SFT requires larger SNR than the FFT and the RSFT based methods. In near range radar applications, such as automotive radar, high SNR is relatively easy to obtain.

V. CONCLUSION

In this paper, we have proposed RFPS-SFT, a robust extension of the SFT algorithm based on Fourier projection-slice theorem. We have shown that RFPS-SFT can address multidimensional data that contains off-grid frequencies and noise, while enjoys low complexity. Hence the proposed RFPS-SFT is suitable for the low-complexity implementation of multidimensional DFT based signal processing, such as the signal processing in DBF automotive radar.

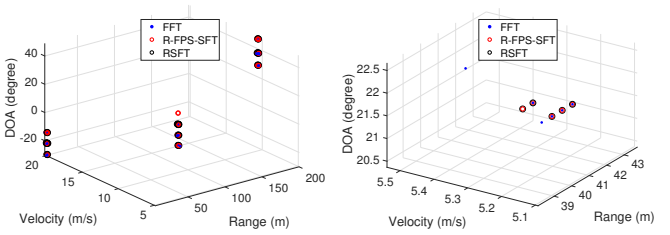

(a) (b)

Fig. 5. Radar target reconstruction via FFT, FPS-SFT and RSFT. (a) Reconstruction of three targets. (b) Details of the frequency locations that are reconstructed for one of the three targets.

ACKNOWLEDGEMENT

The work was supported by ARO grant W911NF-16-1-0126, NSF Grant ECCS-1408437, China Scholarship Council and Shanghai Institute of Spaceflight Electronics Technology.

REFERENCES

[1] M. Schneider, "Automotive radar-status and trends," in *German microwave conference*, pp. 144–147, 2005.

[2] K. Shirakawa, S. Kobashi, Y. Kurono, M. Shono, and O. Isaji, "3d-scan millimeter-wave radar for automotive application," *Fujitsu Ten Tech. J*, vol. 38, pp. 3–7, 2013.

[3] F. Engels, P. Heidenreich, A. M. Zoubir, F. K. Jondral, and M. Wintermantel, "Advances in automotive radar: A framework on computationally efficient high-resolution frequency estimation," *IEEE Signal Processing Magazine*, vol. 34, no. 2, pp. 36–46, 2017.

[4] H. Hassanieh, P. Indyk, D. Katabi, and E. Price, "Nearly optimal sparse Fourier transform," in *Proceedings of the forty-fourth annual ACM symposium on Theory of computing*, pp. 563–578, ACM, 2012.

[5] A. C. Gilbert, P. Indyk, M. Iwen, and L. Schmidt, "Recent developments in the sparse Fourier transform: A compressed Fourier transform for big data," *Signal Processing Magazine, IEEE*, vol. 31, no. 5, pp. 91–100, 2014.

[6] S. Pawar and K. Ramchandran, "FFAST: An algorithm for computing an exactly k-sparse DFT in O(klogk) time," *IEEE Transactions on Information Theory*, vol. PP, no. 99, pp. 1–1, 2017.

[7] H. Hassanieh, M. Mayzel, L. Shi, D. Katabi, and V. Y. Orekhov, "Fast multi-dimensional NMR acquisition and processing using the sparse FFT," *Journal of Biomolecular NMR*, pp. 1–11, 2015.

[8] S. Wang, V. M. Patel, and A. Petropulu, "A robust sparse fourier transform and its application in radar signal processing," *IEEE Transactions on Aerospace and Electronic Systems*, 2017.

[9] B. Ghazi, H. Hassanieh, P. Indyk, D. Katabi, E. Price, and L. Shi, "Sample-optimal average-case sparse Fourier transform in two dimensions," in *Communication, Control, and Computing (Allerton), 2013 51st Annual Allerton Conference on*, pp. 1258–1265, IEEE, 2013.

[10] L. Shi, H. Hassanieh, A. Davis, D. Katabi, and F. Durand, "Light field reconstruction using sparsity in the continuous Fourier domain," *ACM Transactions on Graphics (TOG)*, vol. 34, no. 1, p. 12, 2014.

[11] S. Wang, V. M. Patel, and A. Petropulu, "FPS-SFT: A Multi-dimensional Sparse Fourier Transform Based on the Fourier Projection-slice Theorem," Submitted to ICASSP 2018. Avaliable at: http://eceweb1.rutgers.edu/ cspl/publications/fps-sft-multi.pdf.

[12] J. O. Smith and X. Serra, *PARSHL: An analysis/synthesis program for non-harmonic sounds based on a sinusoidal representation*. CCRMA, Department of Music, Stanford University, 1987.

[13] M. I. Skolnik, *Radar handbook*. McGraw-Hill Education, 3rd ed., 2008.